Supporting Information for

Crystallographic Characterization of Lu_2C_{2n} ($2n$ = 76-90): Cluster Selection by Cage Size

Wangqiang Shen,[a] Lipiao Bao,[a] Shuaifeng Hu,[a] Le Yang,[b] Peng Jin,*[b] Yunpeng Xie,*[a] Takeshi Akasaka[a] and Xing Lu*[a]

[a] *State Key Laboratory of Materials Processing and Die & Mould Technology, School of Materials Science and Engineering, Huazhong University of Science and Technology, 1037 Luoyu Road, Wuhan, 430074 China. E-mail:* lux@hust.edu.cn.

[b] *School of Materials Science and Engineering, Hebei University of Technology, Tianjin, 300130 China. E-mail:* china.peng.jin@gmail.com

Table of Contents

(Occ., *e*), NPA charges and natural electron configuration populations of the two Lu atoms of Lu_2C_{2n} (2n = 76, 78, 80, 84, 86, 88, 90) isomers.

Figure S11. Optimized structures of low-energy Lu_2C_{76} isomers with relative energies (kcal/mol) and HOMO-LUMO gap energies (eV, in parenthesis).

Figure S12. Optimized structures of low-energy Lu_2C_{78} isomers with relative energies (kcal/mol) and HOMO-LUMO gap energies (eV, in parenthesis).

Figure S13. Optimized structures of low-energy Lu_2C_{80} isomers with relative energies (kcal/mol) and HOMO-LUMO gap energies (eV, in parenthesis).

Figure S14. Optimized structures of low-energy Lu_2C_{84} isomers with relative energies (kcal/mol) and HOMO-LUMO gap energies (eV, in parenthesis).

Figure S15. Optimized structures of low-energy Lu_2C_{86} isomers with relative energies (kcal/mol) and HOMO-LUMO gap energies (eV, in parenthesis).

Figure S16. Optimized structures of low-energy Lu_2C_{88} isomers with relative energies (kcal/mol) and HOMO-LUMO gap energies (eV, in parenthesis).

Figure S17. Optimized structures of low-energy Lu_2C_{90} isomers with relative energies (kcal/mol) and HOMO-LUMO gap energies (eV, in parenthesis).

References.

Isolation of Lu_2C_{2n} (2n = 76, 78, 80, 84, 86, 88, 90) isomers. First, the toluene solution of the extract was separated by using LC-9130NEXT apparatus monitored using a UV detector at 330 nm and a Buckyprep column (20 mm × 250 mm, Cosmosil Nacalai Tesque) with toluene as the mobile phase, and fractions L-1 to L-4 were collected (Figure. S1a). Then, fraction L-1 was reinjected into a Buckyprep M column (20 mm × 250 mm, Cosmosil Nacalai Tesque) for the next separation using toluene as the eluent, and fraction L-1-1 was obtained (Figure S1b). Fraction L-1-1 was then carried out on a 5PYE column (20 mm × 250 mm, Cosmosil Nacalai Tesque) with toluene as the mobile phase, and fraction L-1-1-1 was obtained (Figure S1c). Finally, fraction L-1-1-1 was reinjected into a 5PYE column (20 mm × 250 mm, Cosmosil Nacalai Tesque) with toluene as the mobile phase, $Lu_2@T_d(2)$-C_{76} and $Lu_2@D_{3h}(5)$-C_{78} were finally collected (Figure S1d).

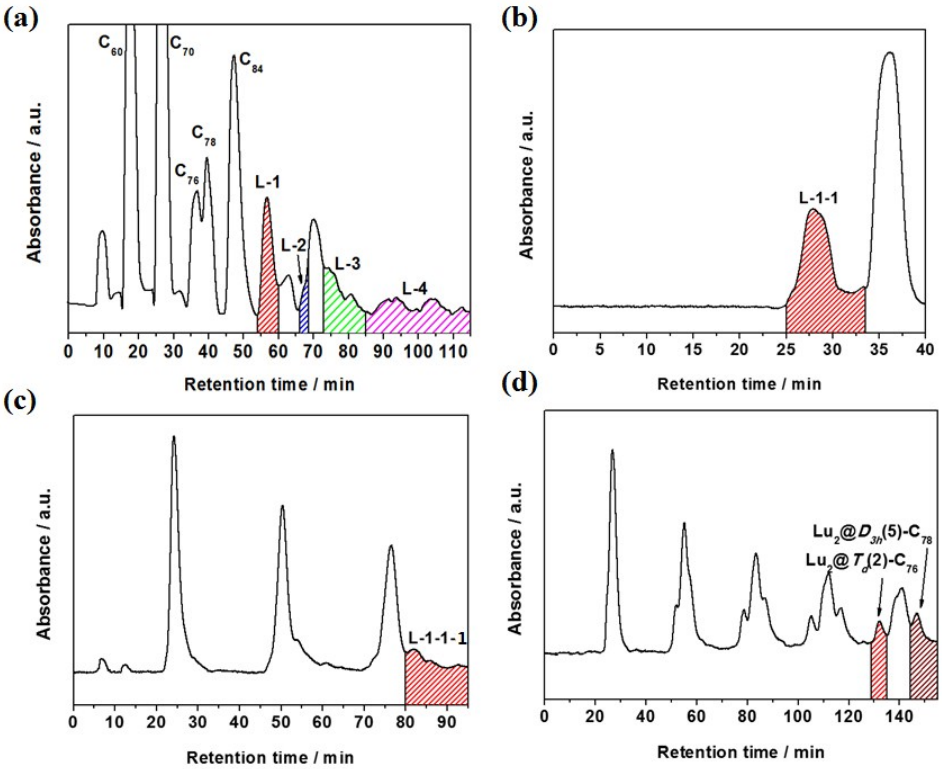

Figure S1. The isolation of $Lu_2@T_d(2)$-C_{76} and $Lu_2@D_{3h}(5)$-C_{78}. HPLC chromatograms of (a) the fullerene extract obtained by a Buckyprep column, (b) fraction L-1 obtained by a Buckyprep M column, (c) fraction L-1-1 obtained by a 5PYE column and (d) $Lu_2@T_d(2)$-C_{76} and $Lu_2@D_{3h}(5)$-C_{78} obtained by a 5PYE column. HPLC conditions: Φ = 20 mm × 250 mm, eluent = toluene, flow rate = 10 mL/min, detection wavelength = 330 nm, room temperature.

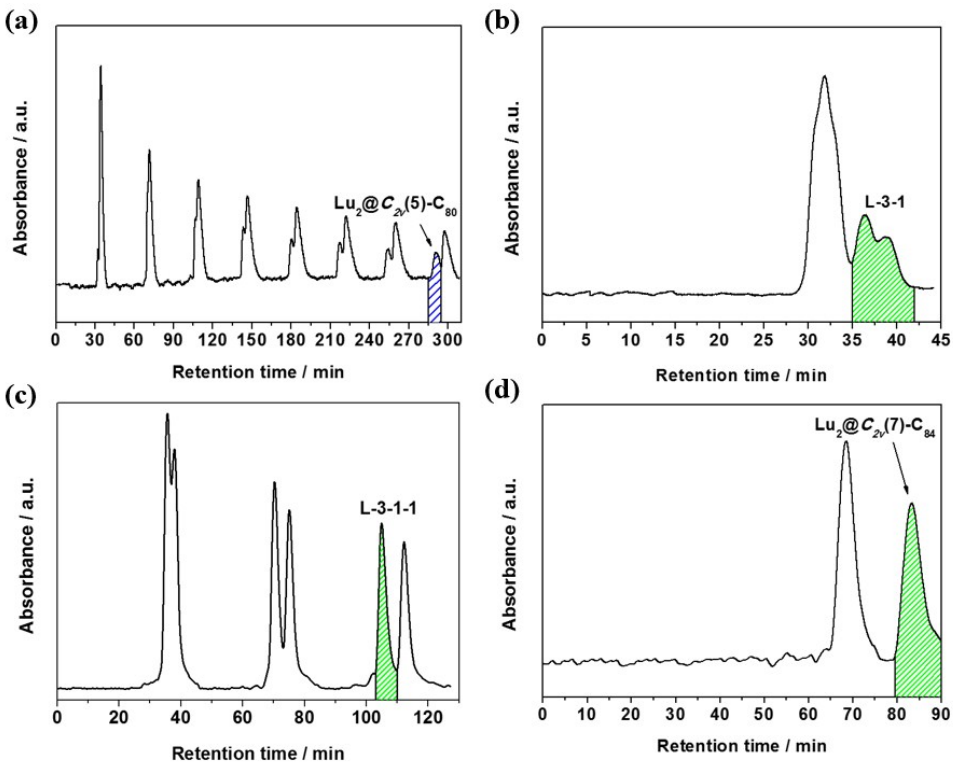

Figure S2. The isolation of $Lu_2@C_{2v}(5)$-C_{80} and $Lu_2@C_{2v}(7)$-C_{84}. (a) HPLC chromatogram of $Lu_2@C_{2v}(5)$-C_{80} obtained by a Buckyprep column with λ = 330 nm, a flow rate of 10 mL/min, and toluene as the eluent at room temperature. (b) HPLC chromatogram of fraction L-3-1 obtained by a Buckyprep M column with λ = 330 nm, a flow rate of 10 mL/min, and toluene as the eluent at room temperature. (c) HPLC chromatogram of fraction L-3-1-1 obtained by a Buckyprep M column with λ = 330 nm, a flow rate of 10 mL/min, and toluene as the eluent at room temperature. (d) HPLC chromatogram of $Lu_2@C_{2v}(7)$-C_{84} obtained by a 5PBB column with λ = 330 nm, a flow rate of 10 mL/min, and chlorobenzene as the eluent at room temperature.

Moreover, fraction L-2 was reinjected into a Buckyprep column (20 mm × 250 mm, Cosmosil Nacalai Tesque) with toluene as the mobile phase, $Lu_2@C_{2v}(5)$-C_{80} was collected (Figure S2a). Fraction L-3 was reinjected into a Buckyprep M column (20 mm × 250 mm, Cosmosil Nacalai Tesque) with toluene as the mobile phase, and fraction L-3-1 was obtained (Figure S2b). Fraction L-3-1 was then carried out on a Buckyprep M column (20 mm × 250 mm, Cosmosil Nacalai Tesque) with toluene as the mobile phase, fraction L-3-1-1 was obtained (Figure S2c). Finally, fraction L-3-1-1 was reinjected into a 5PBB column (20 mm × 250 mm, Cosmosil Nacalai Tesque) with chlorobenzene as the mobile phase, and $Lu_2@C_{2v}(7)$-C_{84} was collected (Figure S2d). Furthermore, fraction L-4 was reinjected into a 5PBB column (20 mm × 250 mm, Cosmosil Nacalai Tesque) with chlorobenzene as the mobile phase, and fractions L-4-1 and L-4-2

were obtained (Figure S3a).

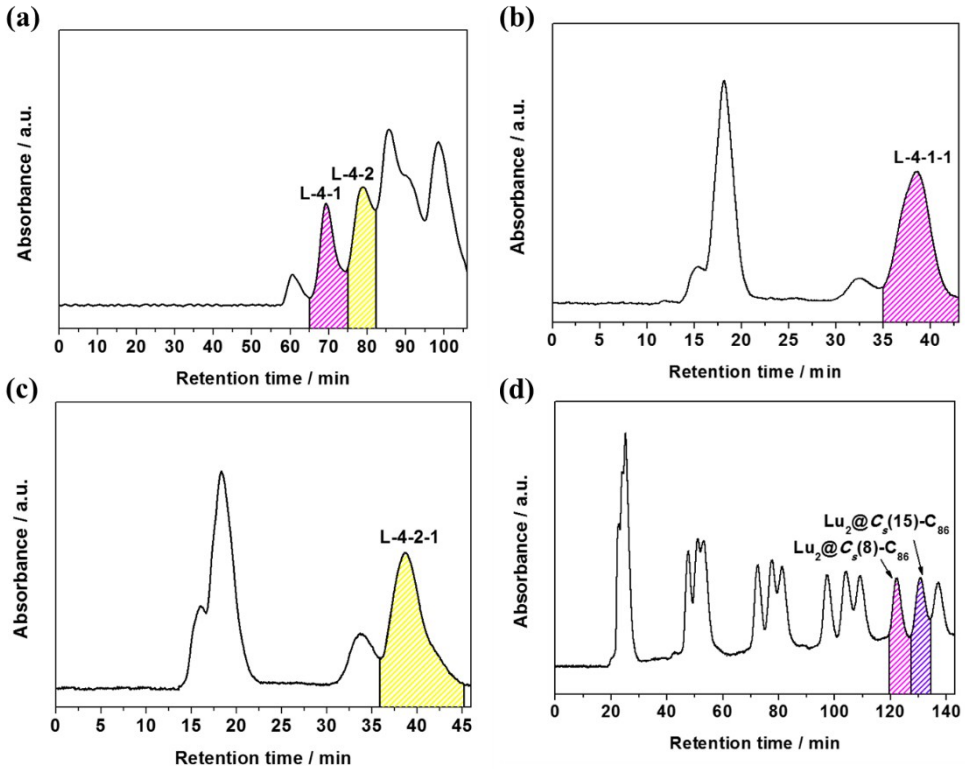

Figure S3. The isolation of $Lu_2@C_s(8)$-C_{86} and $Lu_2@C_s(15)$-C_{86}. HPLC chromatograms of (a) fractions L-4-1 and L-4-2 obtained by a 5PBB column, (b) fraction L-4-1-1 obtained by a Buckyprep M column, (c) fraction L-4-2-1 obtained by a Buckyprep M column and (d) $Lu_2@C_s(8)$-C_{86} and $Lu_2@C_s(15)$-C_{86} obtained by a Buckyprep column. HPLC conditions: Φ = 20 mm × 250 mm, eluent = chlorobenzene, flow rate = 10 mL/min, detection wavelength = 330 nm, room temperature.

Then, fraction L-4-1 was reinjected into a Buckyprep M column (20 mm × 250 mm, Cosmosil Nacalai Tesque) with chlorobenzene as the mobile phase, fraction L-4-1-1 was collected (Figure S3b). Similarly, fraction L-4-2 was then carried out on a Buckyprep M column (20 mm × 250 mm, Cosmosil Nacalai Tesque) with chlorobenzene as the mobile phase, fraction L-4-2-1 was collected (Figure S3c). In the last, fraction L-4-1-1 was carried out on a Buckyprep column (20 mm × 250 mm, Cosmosil Nacalai Tesque) for the next separation using chlorobenzene as the eluent, $Lu_2@C_s(8)$-C_{86} and $Lu_2@C_s(15)$-C_{86} were collected (Figure S3d). Fraction L-4-2-1 was reinjected into a 5PBB column (20 mm × 250 mm, Cosmosil Nacalai Tesque) with chlorobenzene as the mobile phase, and fractions L-4-2-1-1 and L-4-2-1-2 were obtained (Figure S4a). Then, fraction L-4-2-1-1 was reinjected into a 5PBB column (20 mm × 250 mm, Cosmosil Nacalai Tesque) for the next separation using chlorobenzene as the eluent, $Lu_2@C_1(26)$-C_{88} and

$Lu_2C_2@C_{2v}(9)$-C_{86} were collected (Figure S4b). Finally, fraction L-4-2-1-2 was then carried out on a 5PBB column (20 mm × 250 mm, Cosmosil Nacalai Tesque) with chlorobenzene as the mobile phase, $Lu_2C_2@C_s(32)$-C_{88} and $Lu_2C_2@D_2(35)$-C_{88} were collected (Figure S4c).

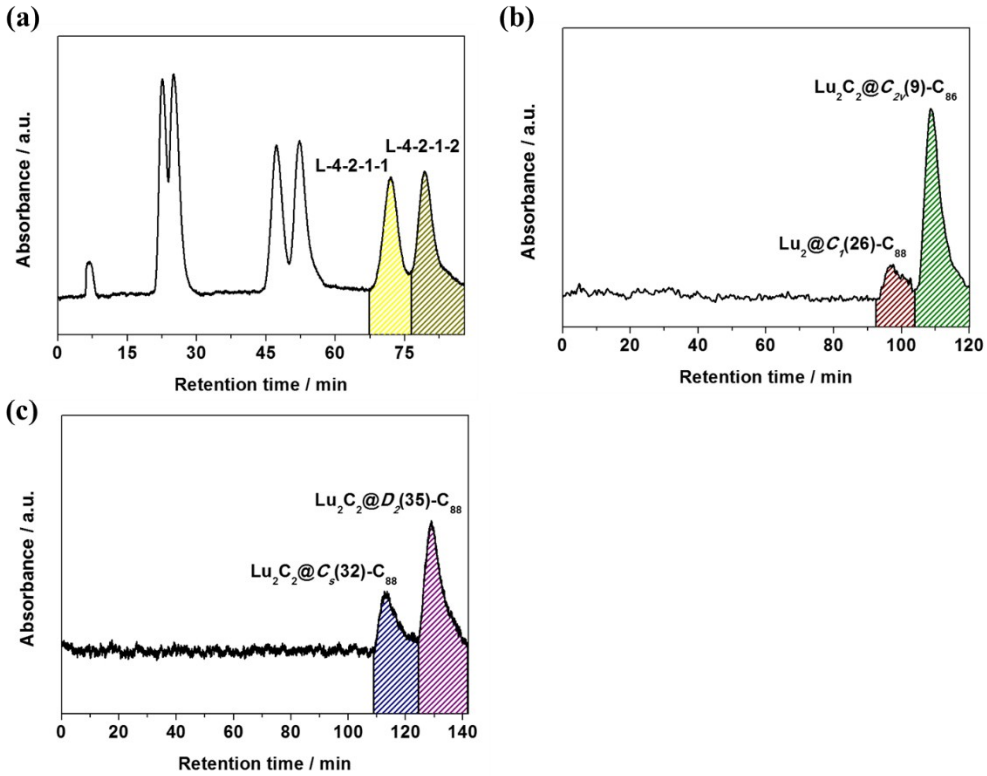

Figure S4. The isolation of $Lu_2@C_1(26)$-C_{88}, $Lu_2C_2@C_{2v}(9)$-C_{86}, $Lu_2C_2@C_s(32)$-C_{88} and $Lu_2C_2@D_2(35)$-C_{88}. HPLC chromatograms of (a) fractions L-4-2-1-1 and L-4-2-1-2 obtained by a Buckyprep column, (b) $Lu_2@C_1(26)$-C_{88} and $Lu_2C_2@C_{2v}(9)$-C_{86} obtained by a 5PBB column and (c) fraction L-1-1-1 obtained by a 5PBB column. HPLC conditions: Φ = 20 mm × 250 mm, eluent = chlorobenzene, flow rate = 10 mL/min, detection wavelength = 330 nm, room temperature.

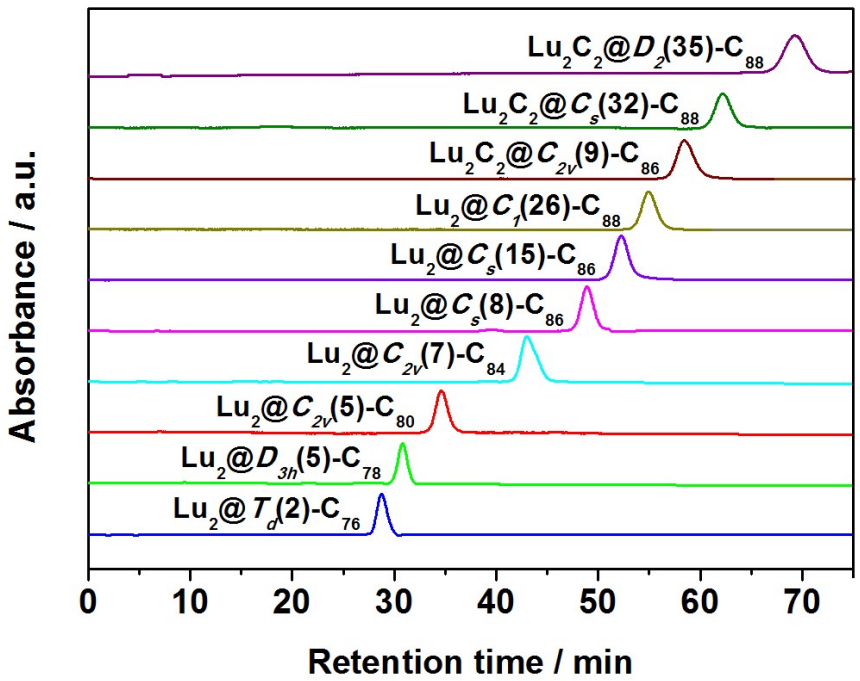

Figure S5. HPLC chromatograms of Lu_2C_{2n} ($2n$ = 76, 78, 80, 84, 86, 88, 90) isomers (HPLC conditions: eluent = toluene, flow rate = 1.0 mL min^{-1}, detection wavelength = 330 nm, room temperature.).

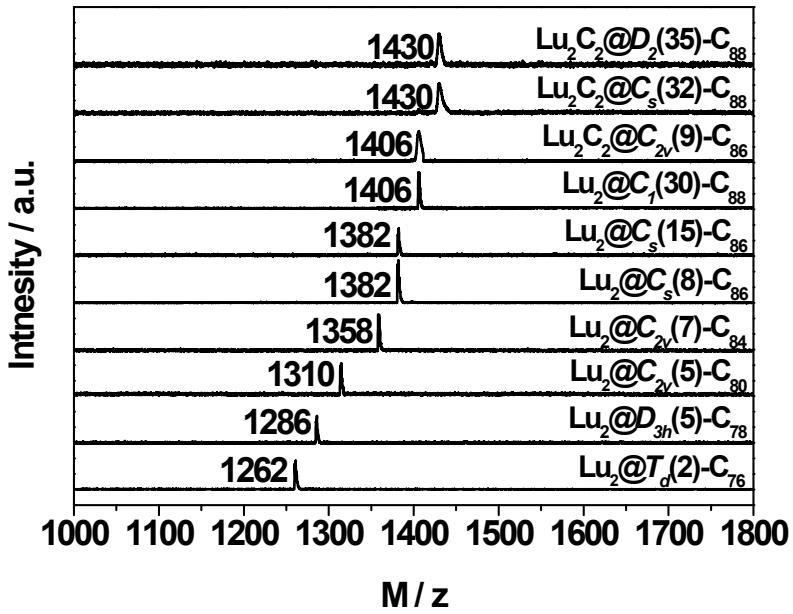

Figure S6. LDI-TOF mass spectra of Lu_2C_{2n} ($2n$ = 76, 78, 80, 84, 86, 88, 90) isomers.

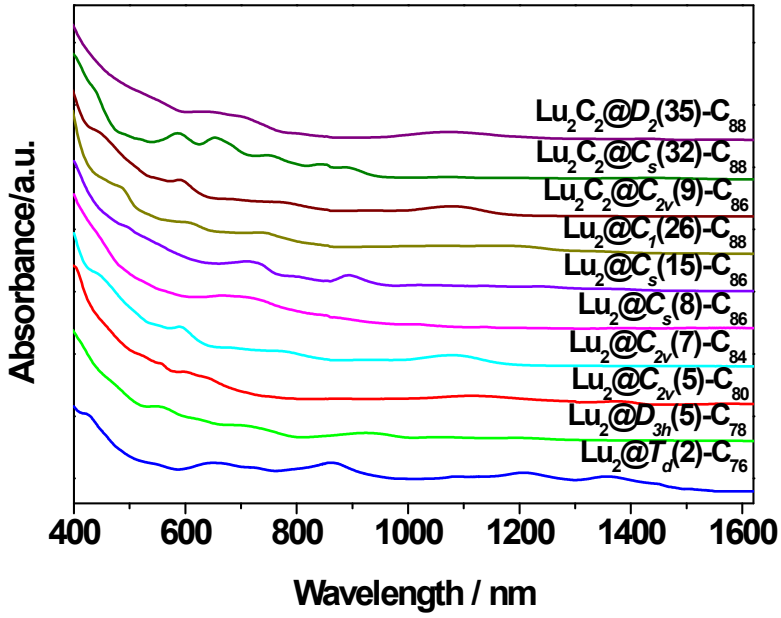

Figure S7. Vis-NIR absorption spectra of Lu_2C_{2n} ($2n$ = 76, 78, 80, 84, 86, 88, 90) isomers.

Table S1. The HPLC retention time and details of the Vis-NIR absorptions of Lu_2C_{2n} (2n = 76, 78, 80, 84, 86, 88, 90) isomers.

EMFs	HPLC retention time (min) [a]	Vis-NIR absorption bands (nm)	Onset (nm)	Optical bandgap (eV)[b]
$Lu_2@T_d(2)$-C_{76}	28.75	545, 643, 726, 852, 1184, 1376	1564	0.79
$Lu_2@D_{3h}(5)$-C_{78}	30.81	460, 561, 637, 726, 934	1098	1.13
$Lu_2@C_{2v}(5)$-C_{80}	34.62	412, 584, 625, 658, 1126, 1389	1488	0.83
$Lu_2@C_{2v}(7)$-C_{84}	42.98	439, 590, 668, 755, 1084	1328	0.93
$Lu_2@C_s(8)$-C_{86}	48.89	480, 664, 706,1015, 1106	1275	0.97
$Lu_2@C_s(15)$-C_{86}	52.25	491, 711, 792, 895, 1234	1448	0.86
$Lu_2@C_1(26)$-C_{88}	54.93	479, 597, 736, 1201	1429	0.87
$Lu_2C_2@C_{2v}(9)$-C_{86}	58.46	433, 591, 678, 776, 932, 1078	1217	1.02
$Lu_2C_2@C_s(32)$-C_{88}	60.21	425, 586, 655, 738, 846, 887	1120	1.11
$Lu_2C_2@D_2(35)$-C_{88}	69.24	630, 707, 804, 1077	1265	0.98

[a]Buckyprep column, flow rate: 1.0 mL/min, eluent: toluene, room temperature.

[b]Optical bandgap (eV) = 1240/onset (nm).

Table S2. The fractional occupancies of the Lu positions in $Lu_2@T_d(2)$-C_{76}, $Lu_2@D_{3h}(5)$-C_{78}, $Lu_2@C_{2v}(5)$-C_{80}, $Lu_2@C_{2v}(7)$-C_{84} and $Lu_2@C_s(8)$-C_{86}.

EMFs	Fractional occupancy of the Lu positions															
	Lu1	Lu2	Lu3	Lu4	Lu5	Lu6	Lu7	Lu8	Lu9	Lu10	Lu11					
$Lu_2@T_d(2)$-C_{76}	0.24	0.21	0.12	0.10	0.10	0.06	0.04	0.04	0.09	0.07	0.02					
	Lu1A	Lu2A	Lu3A	Lu4A	Lu5A	Lu6A	Lu7A	Lu8A								
	0.24	0.21	0.12	0.10	0.10	0.06	0.04	0.04								
	Lu1	Lu2	Lu3	Lu4	Lu5	Lu6	Lu7	Lu8	Lu9							
	0.26	0.13	0.10	0.09	0.07	0.07	0.06	0.38	0.06							
$Lu_2@D_{3h}(5)$-C_{78}	Lu1A	Lu2A	Lu3A	Lu4A	Lu5A	Lu6A	Lu7A									
	0.26	0.13	0.10	0.09	0.07	0.07	0.06									
	Lu1	Lu2	Lu3	Lu4	Lu5	Lu6	Lu7	Lu8	Lu9	Lu10	Lu11	Lu12	Lu13	Lu14	Lu15	Lu16
	0.17	0.11	0.11	0.09	0.08	0.06	0.06	0.05	0.04	0.01	0.02	0.15	0.08	0.07	0.05	0.05
$Lu_2@C_{2v}(5)$-C_{80}											Lu11					
	Lu1A	Lu2A	Lu3A	Lu4A	Lu5A	Lu6A	Lu7A	Lu8A	Lu9A	Lu10A	A					
	0.17	0.11	0.11	0.09	0.08	0.06	0.06	0.05	0.04	0.01	0.02					
	Lu1	Lu2	Lu3	Lu4	Lu5	Lu6	Lu7	Lu8	Lu9	Lu10	Lu11	Lu12	Lu13	Lu14	Lu15	
	0.15	0.15	0.14	0.11	0.08	0.08	0.06	0.06	0.03	0.03	0.02	0.07	0.06	0.04	0.01	
$Lu_2@C_{2v}(7)$-C_{84}											Lu11					
	Lu1A	Lu2A	Lu3A	Lu4A	Lu5A	Lu6A	Lu7A	Lu8A	Lu9A	Lu10A	A					
	0.15	0.15	0.14	0.11	0.08	0.08	0.06	0.06	0.03	0.03	0.02					
	Lu1	Lu2	Lu3	Lu4	Lu5	Lu6	Lu7	Lu8								
	0.31	0.32	0.03	0.12	0.05	0.06	0.24	0.04								
$Lu_2@C_s(8)$-C_{86}	Lu1A	Lu2A	Lu3A	Lu4A	Lu5A											
	0.31	0.32	0.03	0.12	0.05											

Table S3. The fractional occupancies of the Lu positions in $Lu_2@C_s(15)$-C_{86}, $Lu_2@C_1(26)$-C_{88}, $Lu_2C_2@C_{2v}(9)$-C_{86}, $Lu_2C_2@C_s(32)$-C_{88} and $Lu_2C_2@D_2(35)$-C_{88}.

EMFs	Fractional occupancy of the Lu positions															
	Lu1	Lu2	Lu3	Lu4	Lu5	Lu6	Lu7	Lu8	Lu9	Lu10	Lu11					
	0.15	0.13	0.11	0.11	0.09	0.07	0.07	0.05	0.04	0.21	0.15					
$Lu_2@C_s(15)$-C_{86}	Lu1A	Lu2A	Lu3A	Lu4A	Lu5A	Lu6A	Lu7A	Lu8A	Lu9A							
	0.15	0.13	0.11	0.11	0.09	0.07	0.07	0.05	0.04							
	Lu1	Lu2	Lu3	Lu4	Lu5	Lu6	Lu7	Lu8	Lu9	Lu10	Lu11	Lu12	Lu13	Lu14	Lu15	Lu16
	0.27	0.07	0.06	0.06	0.06	0.03	0.03	0.02	0.02	0.02	0.01	0.52	0.07	0.04	0.04	0.03
$Lu_2@C_1(26)$-C_{88}											Lu11					
	Lu1A	Lu2A	Lu3A	Lu4A	Lu5A	Lu6A	Lu7A	Lu8A	Lu9A	Lu10A	A					
	0.27	0.07	0.06	0.06	0.06	0.03	0.03	0.02	0.02	0.02	0.01					
	Lu1	Lu2	Lu3	Lu4	Lu5	Lu6	Lu7	Lu8	Lu9	Lu10	Lu11	Lu12	Lu13			
$Lu_2C_2@C_{2v}(9)$-C_{86}	0.26	0.26	0.26	0.25	0.25	0.24	0.11	0.08	0.08	0.06	0.06	0.05	0.04			
	Lu1	Lu2	Lu3	Lu4	Lu5	Lu6	Lu7	Lu8	Lu9	Lu10	Lu11	Lu12	Lu13	Lu14	Lu15	Lu16
	0.57	0.49	0.22	0.14	0.11	0.10	0.03	0.03	0.03	0.03	0.03	0.02	0.02	0.02	0.02	0.02
$Lu_2C_2@C_s(32)$-C_{88}	Lu17	Lu18	Lu19	Lu20	Lu21	Lu22	Lu23	Lu24								
	0.02	0.02	0.02	0.02	0.01	0.01	0.01	0.01								
	Lu1	Lu2	Lu3	Lu4	Lu5	Lu6	Lu7	Lu8	Lu9							
	0.20	0.19	0.15	0.16	0.11	0.06	0.04	0.13	0.06							
$Lu_2C_2@D_2(35)$-C_{88}	Lu1A	Lu2A	Lu3A	Lu4A	Lu5A	Lu6A	Lu7A									
	0.20	0.19	0.15	0.16	0.11	0.06	0.04									

Table S4. Crystallographic data of $Lu_2@T_d(2)$-C_{76}, $Lu_2@D_{3h}(5)$-C_{78}, $Lu_2@C_{2v}(5)$-C_{80}, $Lu_2@C_{2v}(7)$-C_{84} and $Lu_2@C_s(8)$-C_{86}.

Compounds	**$Lu_2@T_d(2)C_{76}$•$Ni^{II}(OEP)$•2(C_6H_6)**	**$Lu_2@D_{3h}(5)C_{78}$•$Ni^{II}(OEP)$•2(C_6H_6)**	**$Lu_2@C_{2v}(5)C_{80}$•$Ni^{II}(OEP)$•2(C_6H_6)**	**$Lu_2@C_{2v}(7)C_{84}$•$Ni^{II}(OEP)$•(C_6H_6)**	**$Lu_2@C_s(8)C_{86}$•1.5$Ni^{II}(OEP)$•2(C_6H_6)**
T, K	100(2)	100(2)	100(2)	100(2)	173(2)
λ, Å	0.65250	0.65250	0.65250	0.65250	0.71069
color/habit	black / block	black / block	black / block	black / block	black / block
cryst size, mm	0.15×0.10×0.08	0.18×0.12×0.10	0.10×0.10×0.06	0.12×0.08×0.07	0.20×0.12×0.08
empirical formula	$C_{124}H_{56}Lu_2N_4Ni$	$C_{126}H_{56}Lu_2N_4$ Ni	$C_{128}H_{56}Lu_2N_4Ni$	$C_{126}H_{50}Lu_2N_4Ni$	$C_{292}H_{144}Lu_4N_{12}Ni3$
fw	2010.37	2034.39	2058.41	2028.35	4696.19
cryst system	monoclinic	monoclinic	monoclinic	monoclinic	monoclinic
space group	C2/m	C2/m	C2/m	C2/m	C2/m
a, Å	23.1698(6)	25.274(5)	25.186(5)	25.410(5)	24.454(5)
b, Å	13.7779(4)	14.939(5)	15.099(5)	15.110(5)	18.039(5)
c, Å	18.0308(4)	19.653(5)	19.694(5)	19.917(5)	22.303(5)
α, deg	90	90	90	90	90
β, deg	93.7760(10)	93.796(5)	94.158(5)	94.510(5)	101.767(5)
γ, deg	90	90	90	90	90
V, $Å^3$	5743.5(3)	7404(3)	7470(3)	7623(4)	9632(4)
Z	4	4	4	4	2
ρ, g/cm^3	2.325	1.825	1.830	1.767	1.619
μ, mm^{-1}	3.044	2.362	2.342	2.294	2.388
R1 (all data)	0.0921	0.0928	0.1125	0.0818	0.1314
wR2 (all data)	0.2408	0.2807	0.3111	0.2438	0.3535

Table S5. Crystallographic data of $Lu_2@C_s(15)$-C_{86}, $Lu_2@C_1(26)$-C_{88}, $Lu_2C_2@C_{2v}(9)$-C_{86}, $Lu_2C_2@C_s(32)$-C_{88} and $Lu_2C_2@D_2(35)$-C_{88}.

Compounds	**$Lu_2@C_s(15)C_{86}$•**	**$Lu_2@C_1(26)$-C_{88}•**	**$Lu_2C_2@C_{2v}(9)$-C_{86}•**	**$Lu_2C_2@C_s(32)$-C_{88}•**	**$Lu_2C_2@D_2(35)$-C_{88}•**
	$Ni^{II}(OEP)$•2(C_6H_6)	**$Ni^{II}(OEP)$•2(C_6H_6)**	**$Ni^{II}(OEP)$•(C_6H_6)**	**$Ni^{II}(OEP)$•1.6(C_6H_6) •0.4(CS_2)**	**1.5$Ni^{II}(OEP)$•2(C_6H_6)**
T, K	173(2)	100(2)	173(2)	100(2)	100(2)
λ, Å	0.71069	0.65250	0.71069	0.65250	0.65250
color/habit	black / block	black / block	black / block	black / block	black / block
cryst size, mm	0.18×0.12×0.10	0.12×0.08×0.05	0.18×0.15×0.10	0.15×0.10×0.08	0.12×0.10×0.06
empirical formula	$C_{134}H_{56}Lu_2N_4Ni$	$C_{136}H_{56}Lu_2N_4Ni$	$C_{130}H_{50}Lu_2N_4$ Ni	$C_{136}H_{53.6}Lu_2N_4NiS_{0.8}$	$C_{300}H_{144}Lu_4N_{12}Ni_3$
fw	2130.47	2154.50	2076.39	2177.69	4792.27
cryst system	monoclinic	monoclinic	triclinic	triclinic	monoclinic
space group	C2/m	C2/m	P-1	P-1	C2/m
a, Å	24.149(5)	24.121(5)	14.604(5)	14.749(5)	24.634(5)
b, Å	18.020(5)	18.190(5)	15.012(5)	15.029(5)	17.744(5)
c, Å	18.486(5)	18.497(5)	19.852(5)	19.899(5)	23.328(5)
α, deg	90	90	85.556(5)	84.624(5)	90
β, deg	90.220(5)	90.466(5)	88.966(5)	88.620(5)	103.220(5)
γ, deg	90	90	62.445(5)	62.644(5)	90
V, $Å^3$	8044(4)	8115(4)	3846(2)	3899(2)	9927(4)
Z	4	4	2	2	2
ρ, g/cm^3	1.759	1.763	1.793	1.854	1.603
μ, mm^{-1}	2.736	2.160	2.859	2.264	1.845
R1 (all data)	0.0787	0.0586	0.1047	0.0916	0.0957
wR2 (all data)	0.2363	0.1530	0.2816	0.2637	0.2911

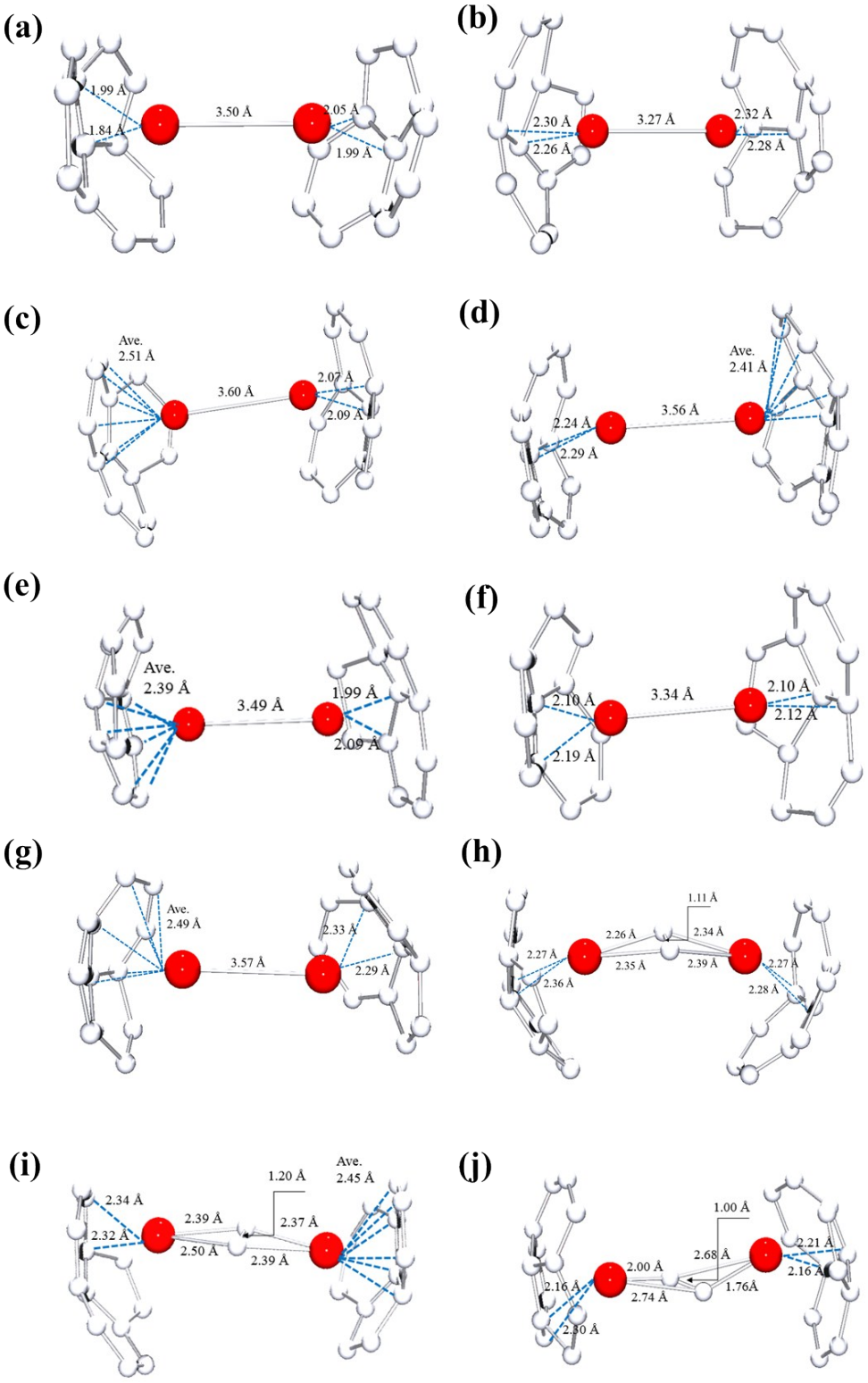

Figure S8. Relative positions of the major Lu_2/Lu_2C_2 cluster to a partial region of the fullerene cage in (a)

$Lu_2@T_d(2)$-C_{76}, (b) $Lu_2@D_{3h}(5)$-C_{78}, (c) $Lu_2@C_{2v}(5)$-C_{80}, (d) $Lu_2@C_{2v}(7)$-C_{84}, (e) $Lu_2@C_s(8)$-C_{86}, (f) $Lu_2@C_s(15)$-C_{86}, (g) $Lu_2@C_1(26)$-C_{88}, (h) $Lu_2C_2@C_{2v}(9)$-C_{86}, (i) $Lu_2C_2@C_s(32)$-C_{88} and (h) $Lu_2C_2@D_2(35)$-C_{88}.

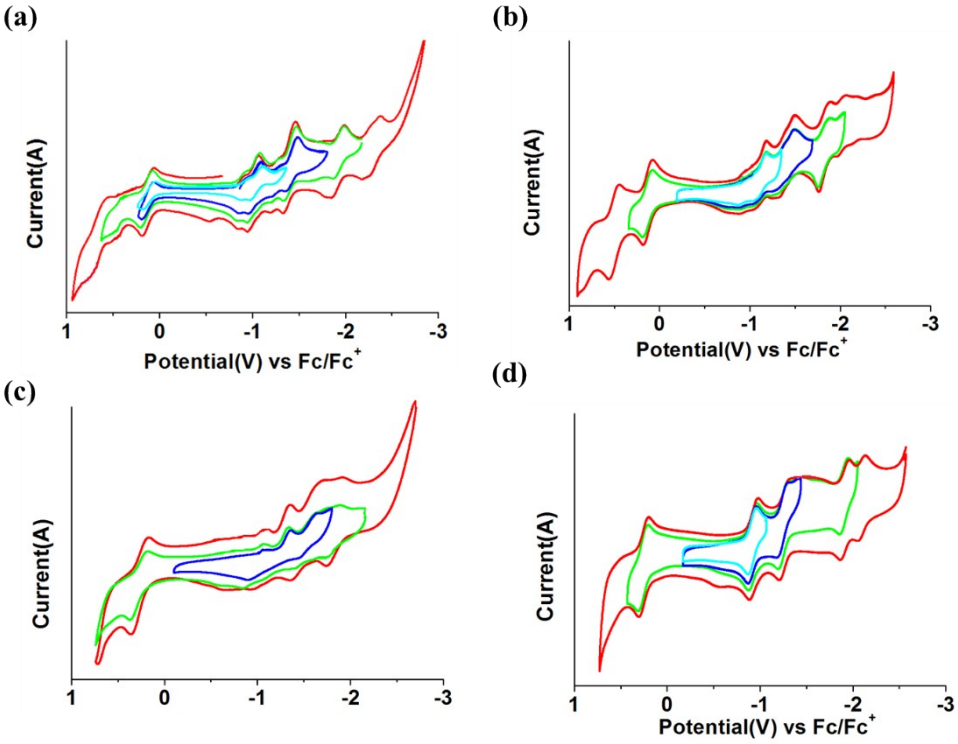

Figure S9. Cyclic voltammogram of (a) $Lu_2@T_d(2)$-C_{76} , (b) $Lu_2@C_{2v}(7)$-C_{84}, (c) $Lu_2@C_s(8)$-C_{86} and (d) $Lu_2@C_s(15)$-C_{86} in 0.05 M n-Bu_4NPF_6/o-DCB solution.

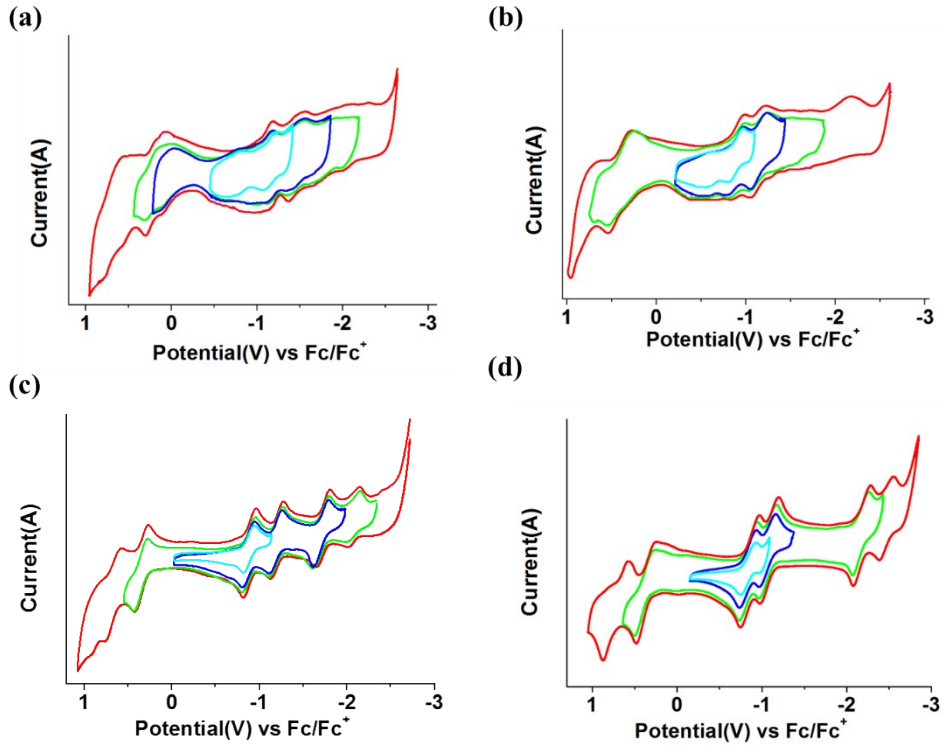

Figure S10. Cyclic voltammogram of (a) $Lu_2@C_1(26)$-C_{88}, (b) $Lu_2C_2@C_{2v}(9)$-C_{86}, (c) $Lu_2C_2@C_s(32)$-C_{88} and (d) $Lu_2C_2@D_2(35)$-C_{88} in 0.05 M n-Bu_4NPF_6/o-DCB solution.

Table S6. Redox potentials[a] (V vs Fc/Fc^+) of $Lu_2@T_d(2)$-C_{76}, $Lu_2@C_s(6)$-C_{82},[S1] $Lu_2@C_{2v}(7)$-C_{84}, $Lu_2@C_s(8)$-C_{86}, $Lu_2@C_s(15)$-C_{86}, $Lu_2@C_{2v}(9)$-C_{86},[S1] $Lu_2@C_1(26)$-C_{88}, $Lu_2C_2@C_{2v}(9)$-C_{86}, $Lu_2C_2@C_s(32)$-C_{88} and (d) $Lu_2C_2@D_2(35)$-C_{88}.

Compounds	$^{ox}E_2$	$^{ox}E_1$	$^{red}E_1$	$^{red}E_2$	$^{red}E_3$	$^{red}E_4$	ΔE_{gap}[c]
$Lu_2@T_d(2)$-C_{76}		0.16	-1.02	-1.42[b]	-1.98[b]	-2.37[b]	1.18
$Lu_2@C_s(6)$-C_{82}[S1]	0.59	0.34	-1.02	-1.35	1.69[b]	-2.05[b]	1.36
$Lu_2@C_{2v}(7)$-C_{84}	0.50	0.13	-1.18[b]	-1.48[b]	-1.70[b]	-1.95[b]	1.31
$Lu_2@C_s(8)$-C_{86}		0.27	-0.96[b]	-1.29[b]	-1.65[b]	-1.89[b]	1.23
$Lu_2@C_s(15)$-C_{86}		0.26	-0.93	-1.25	-1.87	-2.04[b]	1.19
$Lu_2@C_{2v}(9)$-C_{86}[S1]		0.31	-1.01	-1.34[b]	-1.61[b]	-2.23[b]	1.32
$Lu_2@C_1(26)$-C_{88}		0.23	-1.06	-1.46	-1.95[b]	-2.12[b]	1.29
$Lu_2C_2@C_{2v}(9)$-C_{86}		0.41	-0.98	-1.22[b]	-1.73[b]	-2.17[b]	1.39

$Lu_2C_2@C_s(32)$-C_{88}	0.67	0.35	-0.89	-1.15	-1.70	-2.07	1.24
$Lu_2C_2@D_2(35)$-C_{88}	0.72	0.35	-0.86	-1.09	-2.17	-2.47	1.21

[a]Half-wave potentials unless otherwise noted. [b]Peak potentials. [c]$\Delta E_{gap} = {}^{ox}E_1 - {}^{red}E_1$.

Table S7. Interatomic distances ($R_{Lu\text{-}Lu}$, Å), Wiberg bond orders (WBOs), electron occupancies (Occ., *e*), natural population analysis charges and natural electron configuration populations of the two Lu atoms of Lu_2C_{2n} isomers. The Lu atoms are numbered from left to right in Figure 3.

Species	$R_{Lu\text{-}Lu}$	WBO	Occ.	Atom	Charge	Population	hybrid composition
$Lu_2@T_d(2)$-C_{76}	3.44	0.97	1.97	Lu1	0.97	$6s^{0.53}5d^{0.21}6p^{0.65}6d^{0.67}7p^{0.01}$	s(46%)p(37%)d(17%)
				Lu2	0.97	$6s^{0.53}5d^{0.21}6p^{0.65}6d^{0.67}7p^{0.01}$	s(46%)p(37%)d(17%)
$Lu_2@D_{3h}(5)$-C_{78}	3.41	0.98	1.98	Lu1	1.03	$6s^{0.56}5d^{0.38}6p^{0.63}6d^{0.43}7p^{0.01}$	s(49%)p(36%)d(15%)
				Lu2	1.03	$6s^{0.56}5d^{0.38}6p^{0.63}6d^{0.43}7p^{0.01}$	s(49%)p(36%)d(15%)
$Lu_2@C_{2v}(5)$-C_{80}	3.72	0.94	1.97	Lu1	0.99	$6s^{0.57}5d^{0.19}6p^{0.61}6d^{0.65}7p^{0.01}$	s(51%)p(32%)d(17%)
				Lu2	1.08	$6s^{0.56}5d^{0.20}6p^{0.59}6d^{0.59}7p^{0.01}$	s(51%)p(33%)d(16%)
$Lu_2@C_{2v}(7)$-C_{84}	3.46	0.98	1.98	Lu1	1.06	$6s^{0.57}5d^{0.49}6p^{0.62}6d^{0.29}7p^{0.01}$	s(50%)p(35%)d(15%)
				Lu2	1.06	$6s^{0.57}5d^{0.49}6p^{0.62}6d^{0.29}7p^{0.01}$	s(50%)p(35%)d(15%)
$Lu_2@C_s(8)$-C_{86}	3.53	0.96	1.98	Lu1	1.07	$6s^{0.54}5d^{0.20}6p^{0.60}6d^{0.60}7p^{0.01}$	s(48%)p(35%)d(17%)
				Lu2	1.10	$6s^{0.63}5d^{0.19}6p^{0.55}6d^{0.56}7p^{0.01}$	s(55%)p(31%)d(14%)
$Lu_2@C_s(15)$-C_{86}	3.67	0.95	1.97	Lu1	1.11	$6s^{0.68}5d^{0.18}6p^{0.52}6d^{0.53}7p^{0.01}$	s(59%)p(28%)d(13%)

				Lu2	1.10	$6s^{0.52}5d^{0.20}6p^{0.60}6d^{0.60}7p^{0.01}$	s(55%)p(30%)d(15%)
$Lu_2@C_1(26)$-C_{88}	3.65	0.95	1.98	Lu1	1.07	$6s^{0.63}5d^{0.19}6p^{0.54}6d^{0.58}7p^{0.01}$	s(59%)p(28%)d(13%)
				Lu2	1.10	$6s^{0.57}5d^{0.20}6p^{0.57}6d^{0.58}7p^{0.01}$	s(51%)p(33%)d(16%)
$Lu_2C_2@C_{2v}(9)$-C_{86}	4.37	0.17	-	Lu1	1.33	$6s^{0.18}5d^{0.29}6p^{0.49}6d^{0.70}7p^{0.01}$	-
				Lu2	1.33	$6s^{0.18}5d^{0.29}6p^{0.49}6d^{0.70}7p^{0.01}$	-
$Lu_2C_2@C_s(32)$-C_{88}	4.64	0.15	-	Lu1	1.32	$6s^{0.18}5d^{0.42}6p^{0.51}6d^{0.56}7p^{0.01}$	-
				Lu2	1.34	$6s^{0.18}5d^{0.42}6p^{0.49}6d^{0.56}7p^{0.01}$	-
$Lu_2C_2@D_2(35)$-C_{88}	4.64	0.16	-	Lu1	1.33	$6s^{0.19}5d^{0.42}6p^{0.49}6d^{0.56}7p^{0.01}$	-
				Lu2	1.33	$6s^{0.19}5d^{0.42}6p^{0.49}6d^{0.56}7p^{0.01}$	-

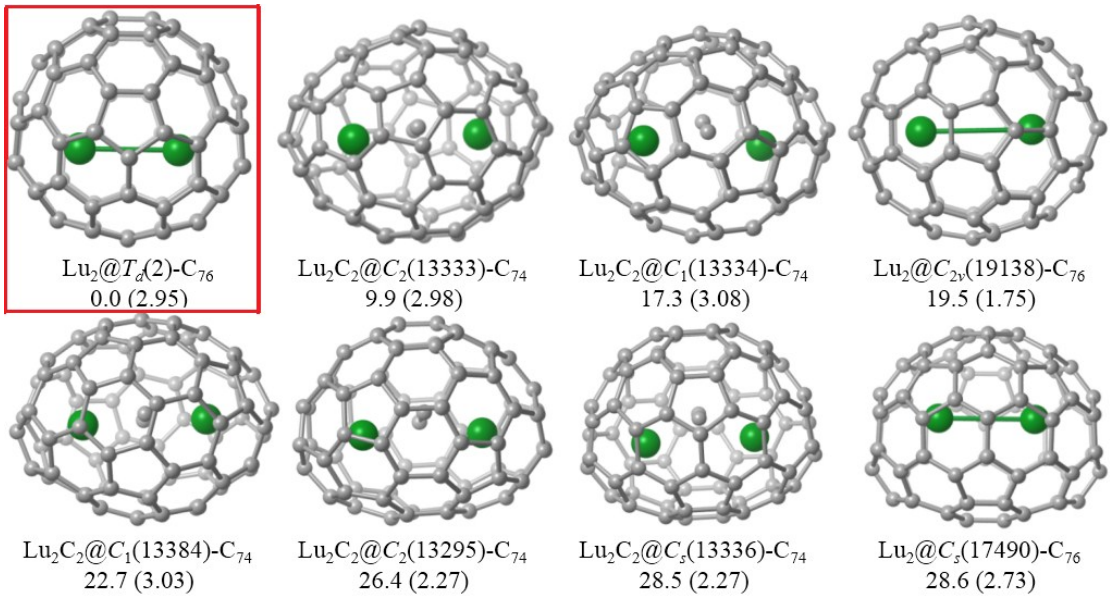

Figure S11. Optimized structures of low-energy Lu_2C_{76} isomers with relative energies (kcal/mol) and HOMO-LUMO gap energies (eV, in parenthesis). The isomer marked with a red box is experimentally obtained.

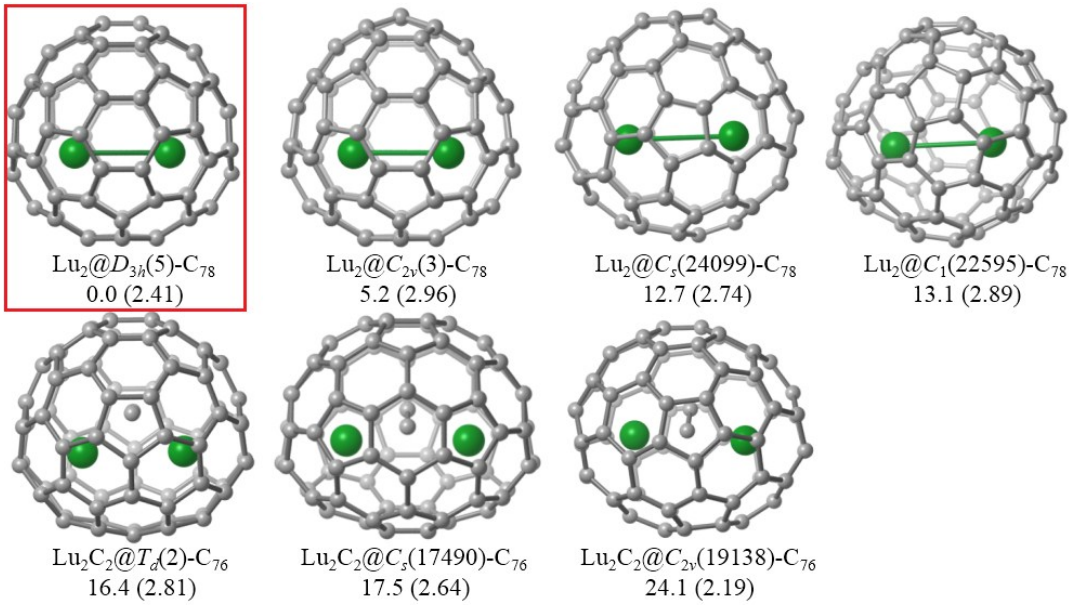

Figure S12. Optimized structures of low-energy Lu_2C_{78} isomers with relative energies (kcal/mol) and HOMO-LUMO gap energies (eV, in parenthesis). The isomer marked with a red box is experimentally obtained.

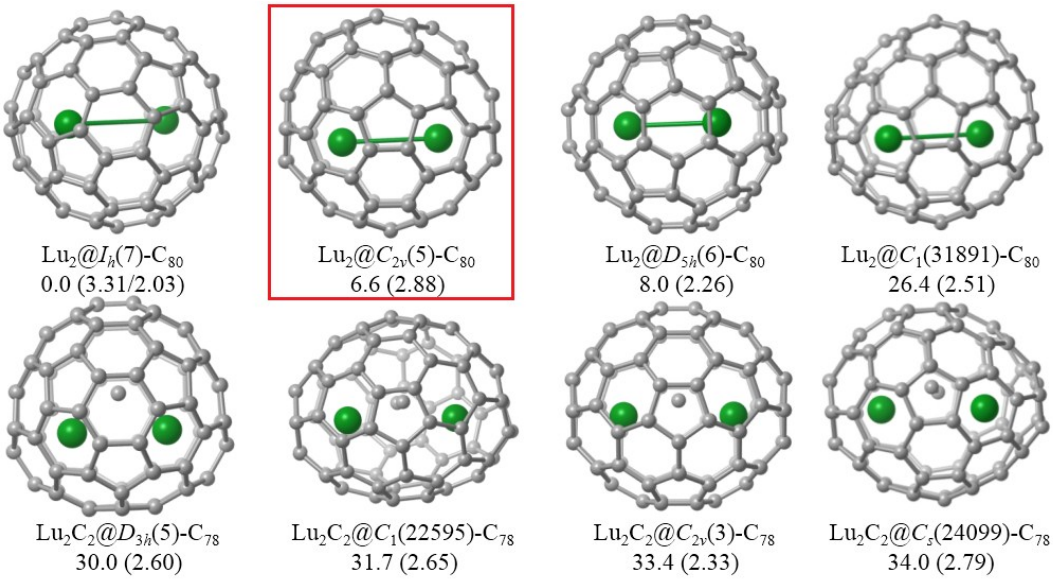

Figure S13. Optimized structures of low-energy Lu_2C_{80} isomers with relative energies (kcal/mol) and HOMO-LUMO gap energies (eV, in parenthesis, α/β for the open-shell ones). The isomer marked with a red box is experimentally obtained.

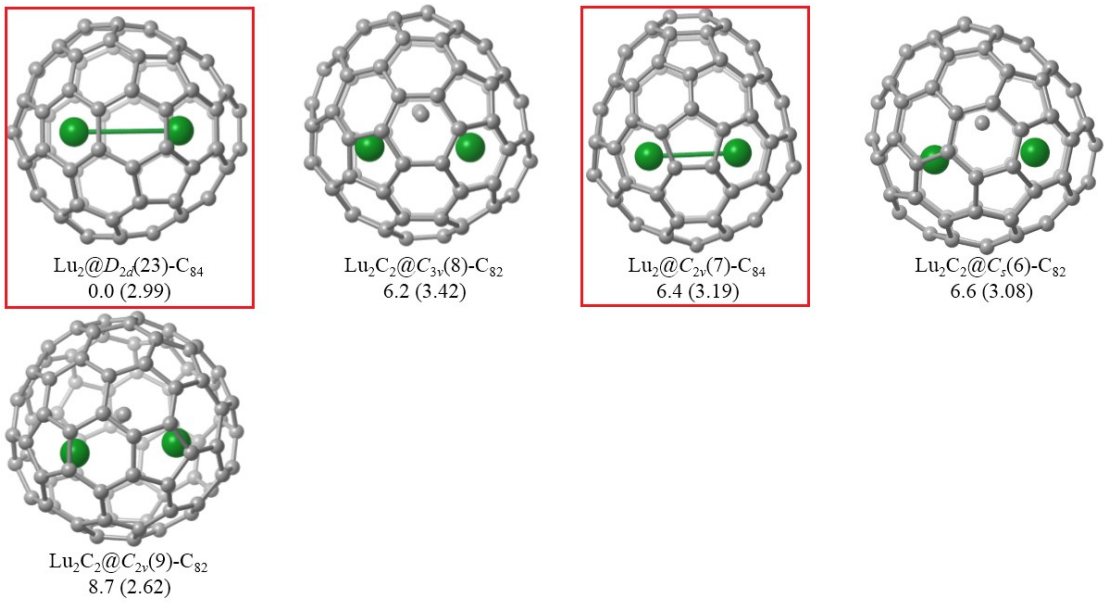

Figure S14. Optimized structures of low-energy Lu_2C_{84} isomers with relative energies (kcal/mol) and HOMO-LUMO gap energies (eV, in parenthesis). The isomers marked with red boxes are experimentally obtained.

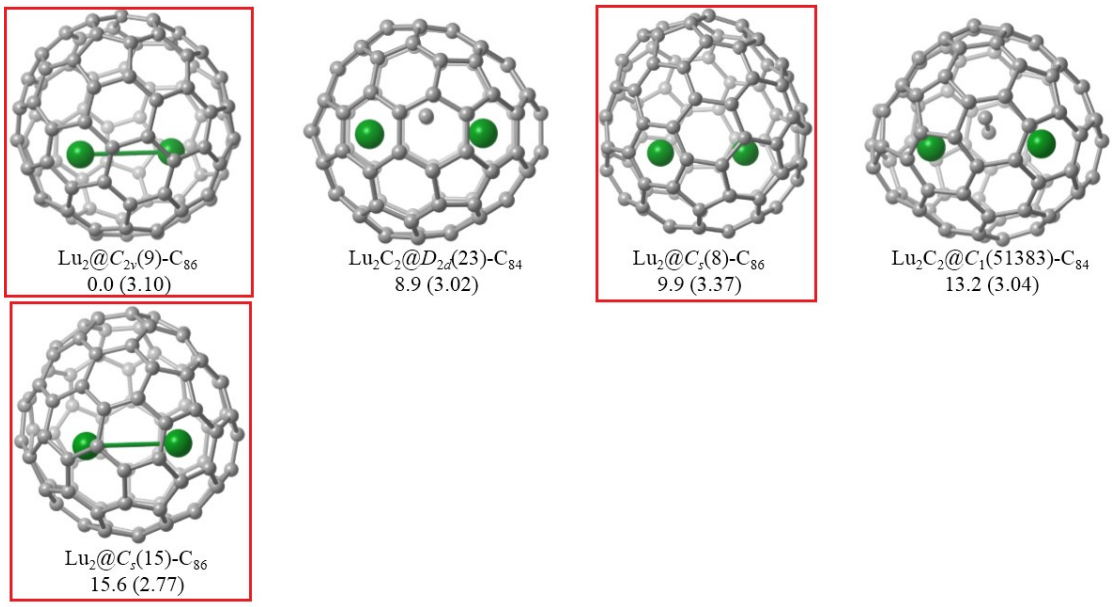

Figure S15. Optimized structures of low-energy Lu_2C_{86} isomers with relative energies (kcal/mol) and HOMO-LUMO gap energies (eV, in parenthesis). The isomers marked with red boxes are experimentally obtained.

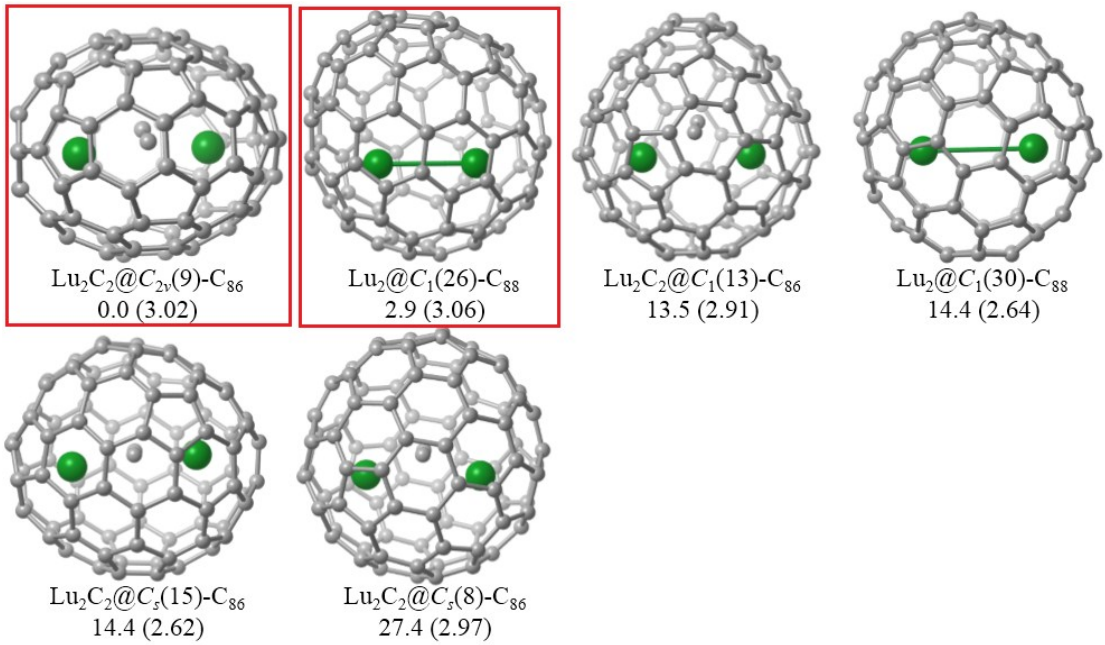

Figure S16. Optimized structures of low-energy Lu_2C_{88} isomers with relative energies (kcal/mol) and HOMO-LUMO gap energies (eV, in parenthesis). The isomers marked with red boxes are experimentally obtained.

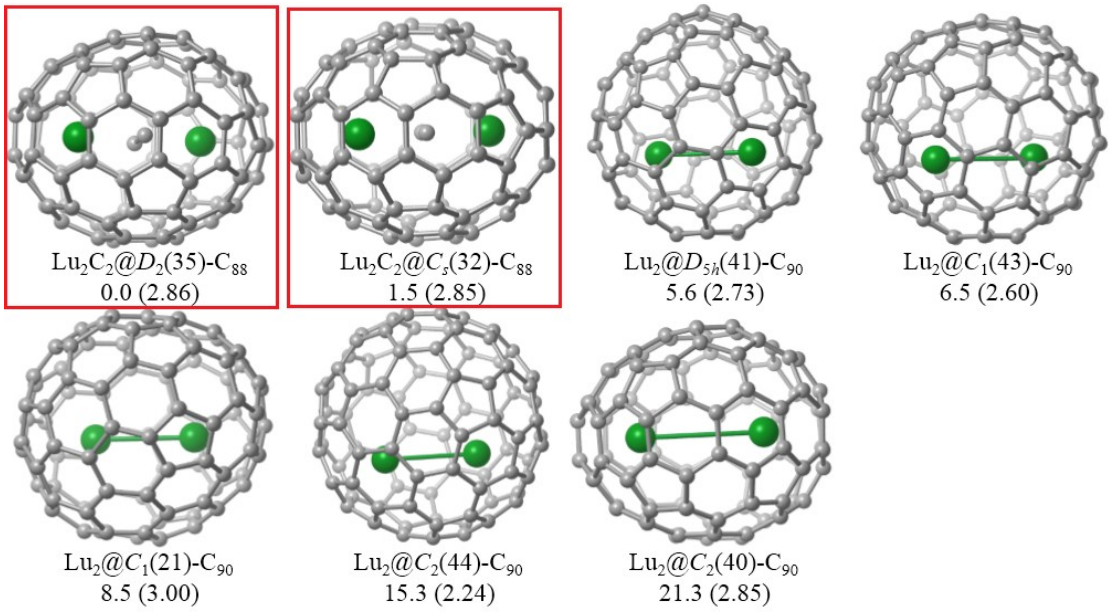

Figure S17. Optimized structures of low-energy Lu_2C_{90} isomers with relative energies (kcal/mol) and HOMO-LUMO gap energies (eV, in parenthesis). The isomers marked with red boxes are experimentally obtained.

References:

[S1]. W. Shen, L. Bao, Y. Wu, C. Pan, S. Zhao, H. Fang, Y. Xie, P. Jin, P. Peng, F.-F. Li and X. Lu, *J. Am. Chem. Soc.*, 2017, **139**, 9979–9984